An Approach to Ideal Semiconductor Electrodes for Efficient Photoelectrochemical Reduction of Carbon Dioxide by Modification with Small Metal Particles

R. Hinogami, Y. Nakamura, S. Yae, and Y. Nakato*

Department of Chemistry, Graduate School of Engineering Science, and Research Center for Photoenergetics of Organic Materials, Osaka University, Toyonaka, Osaka 560-8531, Japan

Received: August 14, 1997; In Final Form: November 10, 1997

Photoelectrochemical reduction of carbon dioxide (CO_2) on p-type silicon (p-Si) electrodes modified with small metal (Cu, Ag, or Au) particles has been studied. The electrodes in CO_2-saturated aqueous electrolyte under illumination produce methane, ethylene, carbon monoxide, etc., similar to the metal (Cu, Ag, or Au) electrodes, but at ca. 0.5 V more positive potentials than the corresponding metal electrodes, contrary to continuous-metal-coated p-Si electrodes. The results clearly show that the metal-particle-coated p-Si electrodes not only have high catalytic activity for electrode reactions but also generate high photovoltages and thus work as an ideal type semiconductor electrode. It is discussed that the CO_2 photoreduction proceeds with an upward shift of the surface band energies of p-Si in order to get energy level matching between the semiconductor and solution reactants, though hydrogen photoevolution occurs without such an upward shift. It is also discussed that the control of surface structure on a nanometer-sized level, as well as on an atomic scale, is important for getting higher efficiencies.

Introduction

Photoelectrochemical (PEC) reduction of carbon dioxide (CO_2) with a p-type semiconductor electrode is one of the solar energy conversion technologies and is important from a viewpoint of the global environmental problems. The method can be regarded as an artificial model for photosynthesis in natural plant and is interesting in this respect.

A number of studies have been made on the PEC reduction of CO_2 on p-type semiconductor electrodes such as p-CdTe,[1−3] p-InP,[3,4] p-GaP,[3,5,6] p-Si,[3,7] p-SiC,[8] etc., with or without metal coating, and some reduction products such as formic acid and carbon monoxide are reported to be produced with relatively high current efficiencies. However, the photovoltage or the solar-to-chemical energy conversion efficiency still remains relatively low. The main reason lies in that it is very difficult to meet all requirements for high efficiency, such as high catalytic activity at the electrode surface, sufficient passivation of the electrode surface (or little surface carrier recombination), formation of a high energy barrier at the semiconductor/solution interface, and good energy level matching between semiconductor and solution reactants for little energy losses in interfacial reactions. The difficulty is serious because the above requirements are not necessarily compatible with each other for most semiconductor electrodes. For example, the first and the second requirements are incompatible because catalytically active surface sites usually act as effective surface recombination centers. They also produce surface states which may cause Fermi level pinning leading to a low energy barrier height.

We have found, through studies of n-Si-based PEC solar cells,[9,10] that a semiconductor electrode modified with small metal particles (e.g., *n*-Si modified with a Langmuir−Blodgett layer of colloidal Pt particles[11,12]) can meet all the requirements mentioned above and thus becomes an ideal type semiconductor electrode. This principle was applied successfully to hydrogen photoevolution on platinum-particle-modified p-Si[13] and p-InP.[14] The purpose of the present paper is to study the PEC reduction of CO_2 on metal (Cu, Ag, or Au) particle-modified p-Si electrodes (cf. Figure 1) and investigate how efficiently the electrodes of this type work for such a slow reaction as the CO_2 reduction with a high activation energy. The Cu, Ag, and Au metals were chosen because they were reported to work as efficient electrocatalysts for the CO_2 reduction.[15,16] Parts of preliminary results were reported in a letter[17] and a short paper.[18]

Experimental Section

Single-crystal p-Si wafers [CZ, (100), 1.3−1.75 Ω cm, or (111), 0.85−1.05 Ω cm, Shin-Etsu Handotai Co., Ltd.] were cut into pieces (about 1.0 × 1.0 cm^2 in area), washed with boiling acetone to remove organic contamination on the surface, etched in CP-4A (a mixture of 47% HF, 60% HNO_3, 99.7% CH_3COOH, and H_2O in a volume ratio of 3:5:3:22), and finally etched again with 12% HF. Ohmic contact was made on the rear side of the Si piece with indium−gallium−zinc alloy. The p-Si piece thus obtained was placed in a Teflon holder and used as a p-Si electrode (effective area: 0.25 or 0.50 cm^2).

Copper (Cu) particles were deposited on p-Si in 0.01 M $CuSO_4$ + 0.18 M H_2SO_4 (M = mol/dm^3) under illumination with a tungsten−halogen lamp, with the potential kept at −0.1 V vs SCE. The current density decreased initially from ca. 5.0 to ca. 0.8 mA/cm^2 but became constant in ca. 30 s. Ag and Au particles were deposited similarly at 0.0 V vs SCE in 0.01 M $AgNO_3$ + 0.66 M HNO_3 and in 0.01 M $HAuCl_4$, respectively. The electricity passing across the electrode surface was measured with a Coulomb meter for all the cases and regulated such that the volume of the deposited metal was nearly the same ($(2.7−3.0) \times 10^{-12}$ m^3) among the Cu, Ag, and Au metals. In other words, the electricity was regulated to be 80, 28, and 80 mC/cm^2 for the Cu, Ag, and Au deposition, respectively, by taking account of the differences in the lattice constant of the metals and the number of electrons needed to reduce one metal ion. For comparison, continuous-metal layers were deposited

S1089-5647(97)02663-1 CCC: $15.00
Published on Web 01/22/1998

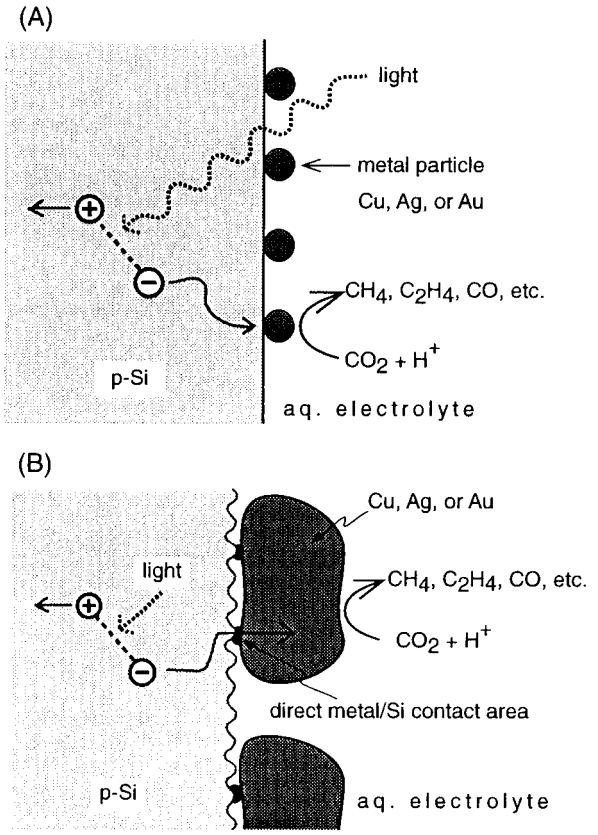

Figure 1. Schematic cross sections of p-Si electrodes coated with small metal particles, together with some electronic processes at the surface: (A) model electrode and (B) actual electrode. See the Discussion section for details.

on p-Si by the vacuum evaporation method under a pressure less than 1×10^{-5} Torr (1 Torr = 133.3 Pa). Chips of Cu (99.994% in purity), Ag (>99.95%), and Au (99.99%) were used as a target. The thickness of the metal layer was monitored with a quartz oscillator placed perpendicular to the direction of the evaporated metal vapor. The thickness was regulated to be 10−30 nm.

Copper metal electrodes were prepared using Cu rod (99.999%) or Cu sheet (99.994%). They were in some cases electrochemically polished at 2.0 V vs a Cu-plate counter electrode in 85.0% phosphoric acid for ca. 1 min. Silver electrodes, made of Ag plate (99.99%), were etched with a mixture of 60% HNO_3 and methanol (volume ratio 1:9). Gold electrodes, made of Au plate (99.99%), were etched with aqua regia.

The PEC reduction of CO_2 was performed using an H-shaped Pyrex cell, with a saturated calomel electrode (SCE) as the reference electrode and a Pt plate as the counter electrode. The cathode and anode compartments were separated with a cation exchange membrane (Nafion 117) in order to avoid mixing of products at the cathode and the anode. The electrolyte was aqueous 0.1 M $KHCO_3$. Current−potential ($j-U$) curves were measured with a potentiostat (Nikko-Keisoku NPOT-2501) and a function generator (Hokutodenko HB-III). The ohmic (iR) drop in the electrolyte (0.1 M $KHCO_3$) between the cathode and SCE, reaching ca. 0.5 V at 10 mA/cm^2, was corrected by measuring the solution resistance by an iR compensation instrument (Hokutodenko HI-203). A tungsten−halogen lamp was used as the light source. The illumination intensity was adjusted such that it gave nearly the same photocurrent as illumination with a solar simulator (AM 1.5 G 100 mW/cm^2, Wacom WXS-85H) for easy comparison with reported solar-cell characteristics.[9−12]

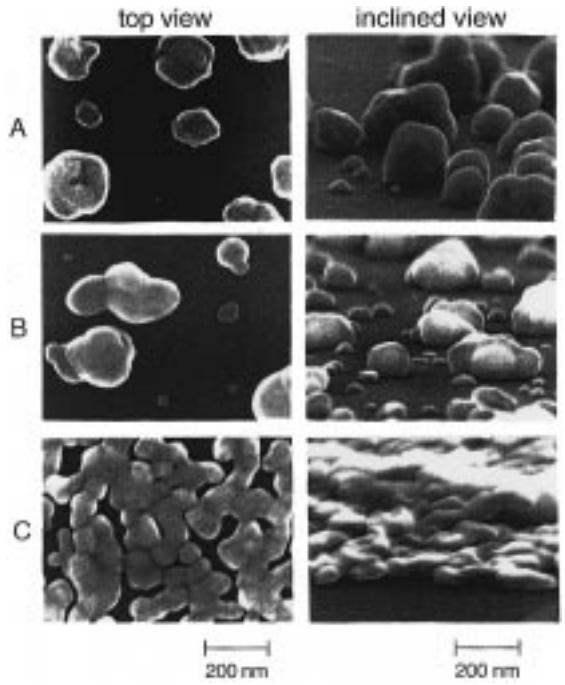

Figure 2. Scanning electron micrographs of p-Si with photoelectrochemically deposited metals: (A) Cu, (B) Ag, and (C) Au.

The $j-U$ curves for the CO_2 photoreduction were measured under continuous bubbling of CO_2 (99.99% in purity) through the catholyte under magnetic stirring, but photoelectrolyses for product analyses were performed under a sealed condition; namely, CO_2 was first bubbled into the stirred catholyte until the air in the cathode compartment was completely substituted for CO_2, then the cathode compartment was sealed, and the photoelectrolysis was carried out potentiostatically under stirring for a certain period of time with recording of the current density. The temperature of the catholyte was kept at 20 ± 1 °C. To remove heavy metal ions contained as impurities in the catholyte, it was beforehand purified by preelectrolysis with a Pt-black electrode at −0.7 V vs SCE for more than 15 h under a N_2 atmosphere. Special-grade chemicals and water purified with a Milli-Q water purification system (Nihon Millipore Kogyo) were used for all experiments.

Reduction products in the gas phase of the cathode compartment were analyzed by gas chromatography. An active carbon column was used for analysis of CO and hydrocarbons, and a molecular sieve 13X column was used for H_2, N_2, and O_2. Organic acids in the catholyte were analyzed by high performance liquid chromatography, using a TSK-gel SCX(H^+) column (Tosoh). Alcohols in the catholyte were analyzed with gas chromatography using a TSG-1 15% column with a support of Shincarbon A 60-80 (Shinwa Kakou).

The electrode surface was inspected with a high-resolution scanning electron microscope (Hitachi S-5000). The surface composition was analyzed by an X-ray photoelectron spectrometer (XPS, Shimadzu ESCA-1000).

Results

1. Surface Structure of Metal Deposited p-Si. Figure 2 shows scanning electron micrographs (SEMs) of p-Si electrodes coated with photoelectrochemically deposited Cu, Ag, and Au. All metals are deposited in the form of small particles of 20−200 nm in size. The particle density was about 2×10^9 cm^{-2} for Cu and Ag and about 2×10^{10} cm^{-2} for Au, as counted from the SEMs. The Au particles are so dense that they form

aggregates. The inclined SEMs (the right-hand side of Figure 2) show that the particles are not spherical but have a rocky shape. Because the metals were deposited such that their volumes were nearly the same as each other, as mentioned in the preceding section, the difference in the particle density among Cu, Ag, and Au may partly be due to the difference in the particle shape. Another possible reason is efficient hole injection by $AuCl_4^-$ (and Ag^+) ions compared with Cu^{2+} (i.e., efficient reduction of the ions (or efficient deposition of Au and Ag)) accompanied by formation of Si oxide layer as described later, which occurs with no flow of Faradaic current. SEM inspection showed that the increase of the electricity passing across the electrode surface did not affect the particle density, only increasing its size. On the other hand, vacuum-deposited metals existed in the form of nearly continuous layers, contrary to the photoelectrochemically deposited metals.

XPS analysis showed that the p-Si surfaces after the photoelectrochemical deposition of metals were covered with Si oxide layers, the thickness being calculated to be 0.3 ± 0.1 nm for Cu, 0.5 ± 0.2 nm for Ag, and 1.5 ± 0.3 nm for Au according to a reported method.[19] The formation of such Si oxide layers was also observed for p-Si simply immersed in the solutions of Cu^{2+}, Ag^+, and $AuCl_4^-$. This indicates that the metal ions can inject holes into the valence band of p-Si, leading to the Si oxide formation and metal deposition.[20−22] The difference in the oxide thickness is probably due to the difference in the reduction potential of Cu^{2+} (0.10 V vs SCE), Ag^+ (0.56 V vs SCE), and $AuCl_4^-$ (0.76 V vs SCE) ions.

2. Hydrogen Photoevolution on Particulate-Metal/p-Si. Hydrogen evolution on Cu, Ag, and Au occurs more efficiently (i.e., with much less overvoltages) than the CO_2 reduction. Therefore, to investigate how well the metal particles were deposited, we first measured the $j-U$ curves for hydrogen photoevolution on the p-Si electrodes coated with photoelectrochemically deposited metal particles (hereafter denoted as particulate-metal/p-Si electrodes) in 1.0 M HCl (pH 0.2). Figure 3 summarizes the $j-U$ curves for various related electrodes. No correction for the *iR* drop was made in this case, because the 1.0 M HCl solution has a high conductivity and the *iR* drop is negligibly small, contrary to the case of 0.1 M $KHCO_3$ described later.

From a glance at Figure 3, it is clear that the onset potentials of photocurrents for the particulate-metal (Cu, Ag, and Au)/p-Si electrodes (after HF etching for the Ag and Au-coated ones) are much more positive than that for a naked p-Si electrode. Decreased photocurrent densities for the particulate-metal/p-Si electrodes are due to decreases in incident light intensity by the deposited metal particles. Moreover, the onset potentials of photocurrents for the particulate-metal/p-Si electrodes lie much more positive than those for the corresponding metal (Cu, Ag, and Au) electrodes, indicating that high photovoltages are generated in p-Si, and also are 0.20−0.25 V more positive than the equilibrium hydrogen-evolution potential (−0.25 V vs SCE) in 1.0 M HCl (pH 0.2). Poor $j-U$ curves before the HF etching for the particulate-Ag and Au/p-Si (Figure 3) are due to the presence of Si oxide layers for the as-deposited electrodes as already mentioned. A simple immersion in 3% HF for 3 min gives effective $j-U$ curves such as shown in Figure 3.

The p-Si electrodes coated with vacuum-deposited Cu, Ag, and Au layers (denoted as continuous-metal/p-Si in Figure 3) show cathodic currents even in the dark, and the onset potentials are similar to those for the corresponding metal electrodes, quite contrary to the case of the particulate-metal/p-Si electrodes. In particular, the $j-U$ curve for the continuous-Au/p-Si shows no photoeffect and nearly agrees with that for an Au electrode, indicating that the Au/p-Si contact is nearly ohmic. For the continuous-Cu and Ag/p-Si, the dark currents have a tendency of saturation at largely negative potentials, and the currents are increased to some extent by illumination. These results indicate that the Cu/p-Si and Ag/p-Si contacts form only low Schottky barriers. The behavior of the continuous-Cu, Ag, and Au/p-Si electrodes described here is in good agreement with reported barrier heights for contacts between p-Si (or n-Si) and Cu, Ag, and Au.[23−25]

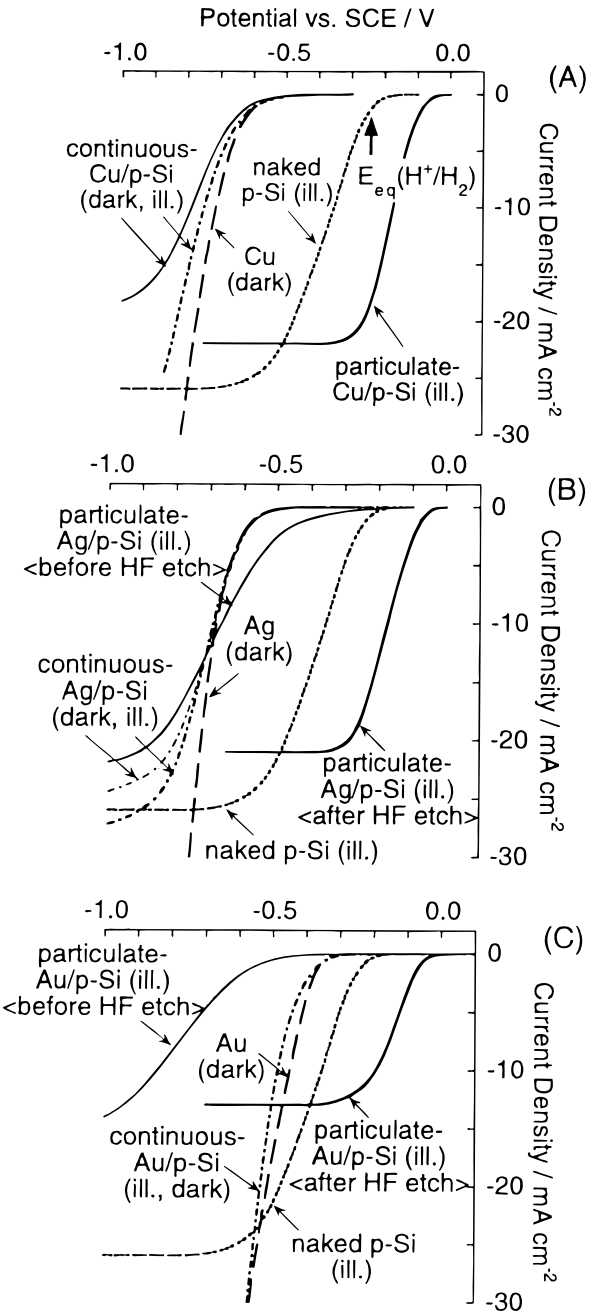

Figure 3. Current-potential ($j-U$) curves for hydrogen evolution in 1.0 M HCl (pH 0.2) at 20 °C: (A) Cu-related electrodes, (B) Ag-related electrodes, and (C) Au-related electrodes. $E_{eq}(H^+/H_2)$ is the equilibrium hydrogen-evolution potential at pH 0.2.

3. CO_2 Photoreduction on Particulate-Metal/p-Si. Figure 4 summarizes the $j-U$ curves for the CO_2 reduction on the particulate-metal/p-Si and other related electrodes in CO_2-saturated aqueous 0.1 M $KHCO_3$ (pH 6.8). It is reported that the solubility of CO_2 in aqueous solution is 38 mM at 25 °C

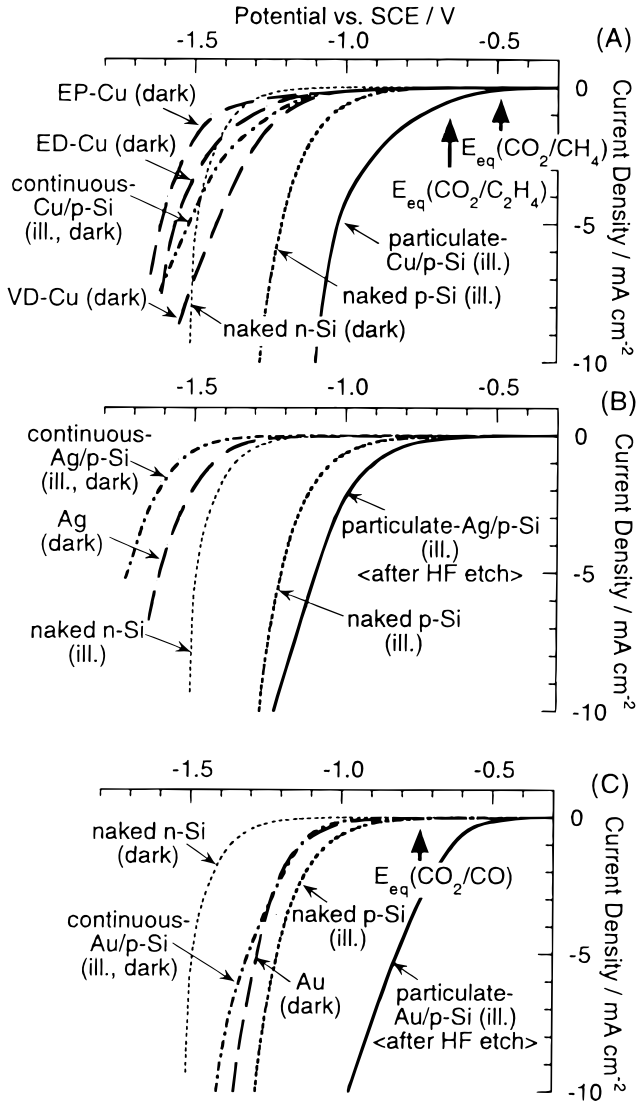

Figure 4. Current-potential ($j-U$) curves for CO_2 reduction in CO_2-saturated aqueous 0.1 M $KHCO_3$ (pH 6.8) at 20 °C: (A) Cu-related electrodes, (B) Ag-related electrodes, and (C) Au-related electrodes. $E_{eq}(CO_2/CH_4)$, $E_{eq}(CO_2/C_2H_4)$, and $E_{eq}(CO_2/CO)$ are the equilibrium potentials for the CO_2 reduction to CH_4, C_2H_4, and CO at pH 6.8, respectively.

and the CO_2 reduction current cannot exceed ~10 mA/cm^2 due to the diffusion limitation.[3] Therefore, only the curves in the region of j less than 10 mA/cm^2 are shown in Figure 4. All the $j-U$ curves in Figure 4 are corrected for the *iR* drop between the working and reference electrodes. The $j-U$ curves for the particulate-Cu/p-Si and other Cu-related electrodes, reported in our previous letter,[17] were not corrected for the *iR* drop and are largely different from the present curves in Figure 4A. A part of the results for particulate-Au/p-Si was reported in a short paper.[18]

Similar to the case of hydrogen evolution (Figure 3), the photocurrent onsets for the particulate-metal (Cu, Ag, and Au)/p-Si electrodes (after the HF etching for the particulate-Ag and Au/p-Si) are much more positive than those for the corresponding metal electrodes. Also the photocurrent onsets for the particulate-Cu and Au/p-Si lie more positive than the equilibrium potentials for the CO_2 reduction to C_2H_4 and CO at pH 6.8, respectively (Figure 4A,C). On the other hand, the $j-U$ curves for the continuous-metal (Cu, Ag, and Au)/p-Si show almost no photoeffect and the current onsets lie in the same potential region as those for the corresponding metal electrodes.

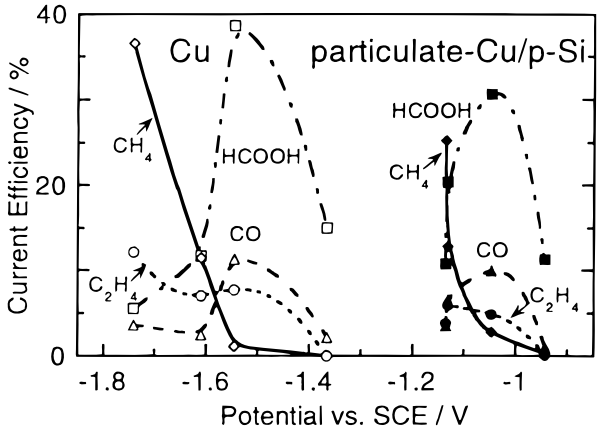

Figure 5. Current efficiencies vs potential for various CO_2-reduction products after potentiostatic electrolyses on particulate-Cu/p-Si and Cu-metal electrodes at 20 °C.

To get accurate photovoltages for the particulate-metal/p-Si electrodes, detailed studies have been made for the Cu-related electrodes. Figure 4A includes the $j-U$ curve for a Cu (99.994%) electrode on which a Cu layer was electrodeposited in the same way as for particulate-Cu/p-Si (denoted by ED-Cu in Figure 4A) and that for a Cu electrode on which a Cu layer was vacuum-deposited in the same way as for continuous-Cu/p-Si (denoted by VD-Cu), together with the curve for a highly pure (99.994%) Cu electrode whose surface was electrochemically polished in 85.0% H_3PO_4 (denoted by EP-Cu). The difference in the $j-U$ curves among ED-Cu, VD-Cu, and EP-Cu suggests that the catalytic activity of Cu is sensitive to the surface structure and impurities.[26−28] The accurate photovoltage for the particulate-Cu/p-Si is thus obtained by comparing the $j-U$ curve for this electrode with that for the ED-Cu electrode. From Figure 4A, we can conclude that the photovoltage is about 0.50 V.

Figure 5 shows the results of product analyses for the CO_2 reduction on the particulate-Cu/p-Si and Cu (99.999%) electrodes in CO_2-saturated 0.1 M $KHCO_3$. The current efficiency for each reduction product is plotted as a function of the electrode potential at which the electrolysis was performed. The *iR* drop between the working and reference electrodes is corrected in Figure 5, similar to the $j-U$ curves in Figure 4, though no correction was made in our previously reported results.[17] The results for the Cu-metal electrode agree well with those reported by Hori et al.[26] and Ito et al.[16] A parallel shift of the current efficiency vs potential curve for each product between the particulate-Cu/p-Si and Cu electrodes by ca. 0.50 V indicates that the Cu particles on p-Si act as an effective catalyst for the CO_2 reduction (cf. Figure 1) with the generation of a high photovoltage of ca. 0.50 V in harmony with the photoshift in the $j-U$ curves of Figure 4A.

Table 1 shows the current efficiencies of reduction products for the particulate-Ag and Au/p-Si electrodes compared with those for Ag, Au, and naked p-Si electrodes. A naked p-Si electrode gave mainly H_2 together with a small amount of CO and HCOOH. The particulate-Ag and Au/p-Si electrodes produced mainly CO, similar to the Ag and Au electrodes,[15,16] but at more positive potentials. Somewhat smaller current efficiencies of CO for the particulate-Ag and Au/p-Si than those for Ag and Au, together with increased current efficiencies of H_2 on the particulate-Ag and Au/p-Si, may suggest that the reduction reactions on the (HF- etched) particulate-Ag and Au/p-Si proceed partly on the naked p-Si surface. The total current efficiency for all the reduction products at each potential does

TABLE 1: Current Efficiencies of Various Reduction Products for Particulate-Ag and Au/p-Si Compared with Those for Ag, Au, and Naked p-Si

electrode	potential [V vs SCE]	current efficiency [%]					j^a [mA/cm^2]	Q^b [C/cm^2]
		H_2	CO	HCOOH	CH_4	C_2H_4		
naked p-Si	−1.27	73.5	12.0	4.3	0.44	0.0	2.40	1.2
Ag	−1.49	14.1	75.9	2.1	0.0	0.0	1.69	10.0
particulate-Ag/p-Si	−1.05	38.4	50.9	0.8	0.0	0.0	2.29	10.0
Au	−1.21	3.7	82.2	0.24	0.0	0.0	2.13	1.6
particulate-Au/p-Si	−0.74	9.0	62.2	0.0	0.0	0.0	1.87	10.0

[a] Average current density during the electrolysis. [b] Electricity which passed during the electrolysis.

not reach unity. This is most probably because the electrolysis experiments were performed in a sealed cell for long periods of time of 1 h and thus parts of the reduction products escaped from the cell (cathode compartment) through the O-ring seals, the cation exchange membrane, etc. However, the essential features of the results shown in Table 1 and Figure 5 were well-reproduced by several-time experiments. Preelectrolysis of the electrolyte did not affect the current efficiencies.

Discussion

As described in the preceding section, a p-Si electrode modified with small metal (Cu, Ag, or Au) particles generates a high photovoltage of ca. 0.5 V and works as an effective electrode for the PEC reduction of CO_2, though a p-Si electrode coated with a continuous metal layer shows almost no photoeffect. Such a sharp contrast clearly shows the prominent effectiveness of particulate-metal coating. Similar sharp contrasts between particulate- and continuous-metal coating were obtained for Pt coated n-Si,[9−12] p-Si,[13] and p-InP,[14] independent of methods of metal deposition and quantities of deposited metal down to a sub-monatomic layer amount,[9] indicating the generality of the result. The mechanism of the efficient CO_2 photoreduction on particulate-metal/p-Si can be explained on the basis of our previously proposed theoretical model for metal-particle-coated n-Si-based solar cells.[9−12]

Let us first consider a *model electrode* such as shown in Figure 1A, the difference from actual electrodes (Figure 2) being discussed later. Metal is deposited sparsely in the form of small particles on p-Si. The ideal size of the areas of direct Si/metal contacts and their separation are estimated theoretically to be about 5 and 20 nm, respectively.[9,10] Photogenerated holes in p-Si enter into the silicon electrode, whereas photogenerated electrons come out to the surface due to the presence of band bending near the p-Si surface. The electrons then transfer into the metal particles and reduce CO_2 at the surface with an aid of catalytic activity of the metal particles. The HF-etched naked p-Si surface is covered with Si−H and Si−OH bonds[29] and passivated.[30] Because the metal particles are small and sparsely distributed, the major part of the p-Si surface is thus kept nearly free from surface states (recombination centers). Moreover, the electrode reactions occur mainly on the metal particles, not on the Si surface, and thus no surface reaction intermediates (surface states and recombination centers) are formed at the Si surface during the electrochemical reactions. Thus, the present type electrode can have high catalytic activity for the electrode reactions and a low surface recombination rate.

Another important point for the present type electrode is that a high (effective) energy barrier is formed at the p-Si/solution contact, irrespective of the intrinsic barrier height for the metal/p-Si contact. The surface band energies of p-Si are more or less modulated by the deposited metal particles and the modulation extends toward the interior of p-Si, as schematically shown in Figure 6, but the modulation is limited spatially only

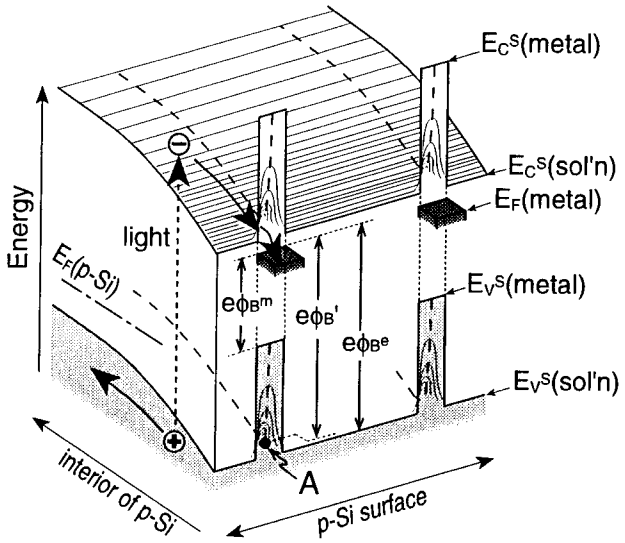

Figure 6. Schematic two-dimensional energy band diagram for a particulate-metal/p-Si electrode under a slight reverse (negative) bias under illumination. E_C^S(metal) and E_V^S(metal) are the bottom of the conduction band and the top of the valence band at the p-Si surface in the area of the direct metal/Si contact, respectively, and E_C^S(soln) and E_V^S(soln) are those in the area of naked p-Si surface, respectively. E_F(metal) and E_F(p-Si) are the Fermi level of metal particles and p-Si, respectively. $e\phi_B^m = E_F(\text{metal}) - E_V^S(\text{metal})$, $e\phi_B^e = E_F(\text{metal}) - E_V^S(\text{soln})$, and $e\phi_B'$ (effective barrier height) is the energy difference between E_F(metal) and the saddle point of the modulated valence band (point A in the figure).

to a region of the same size as the area of the direct metal/Si contact.[9,10] Thus, the effect of the modulation on the barrier height is negligible if the area of the direct metal/Si contact is much smaller than the width of the space charge layer of p-Si. The effective barrier height ($e\phi_B'$ in Figure 6) is then nearly equal to the barrier height for naked p-Si ($e\phi_B^e$) and much higher than the intrinsic barrier height at the direct p-Si/metal contact ($e\phi_B^m$). On the other hand, the barrier height for continuous-metal/p-Si is given by $e\phi_B^m$. A semiconductor electrode coated with homogeneously distributed metal atoms of a sub-monatomic layer amount behaves similar to the continuous-metal-coated electrode.[9]

For the CO_2 photoreduction on the particulate-metal/p-Si electrodes, there remains another notable point. To make it clearer, Figure 7 compares the $j-U$ curves for hydrogen evolution and CO_2 reduction on the particulate-metal/p-Si and metal electrodes. For the hydrogen evolution (Figure 7A), the onset potentials of photocurrents for particulate-Cu, Ag, and Au/p-Si (denoted as Cu, Ag, and Au/p-Si in Figure 7 for simplicity) agree with each other, though the onset potentials for the Cu, Ag, and Au metal electrodes are different from each other. On the contrary, for the CO_2 reduction in Figure 7B, the onset potentials of photocurrents for particulate-Cu, Ag, and Au/p-Si are different from each other, similar to those for the corresponding metal electrodes, yielding a nearly constant

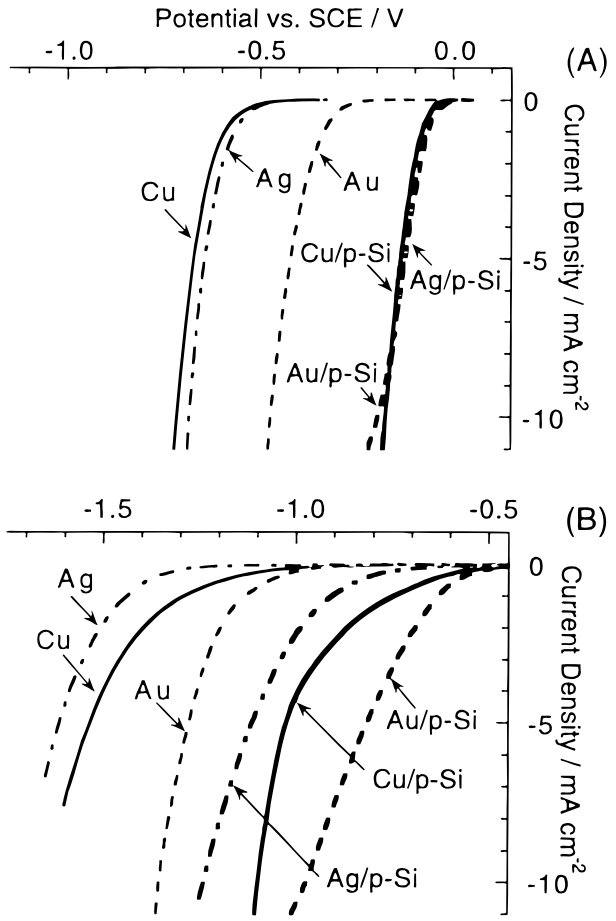

Figure 7. Current-potential ($j-U$) curves of particulate-metal/p-Si (denoted as Cu, Ag, and Au/p-Si in the figures) and metal electrodes; (A) for H_2 evolution in 1.0 M HCl (pH 0.2) and (B) for CO_2 reduction in CO_2-saturated 0.1 M $KHCO_3$ (pH 6.8).

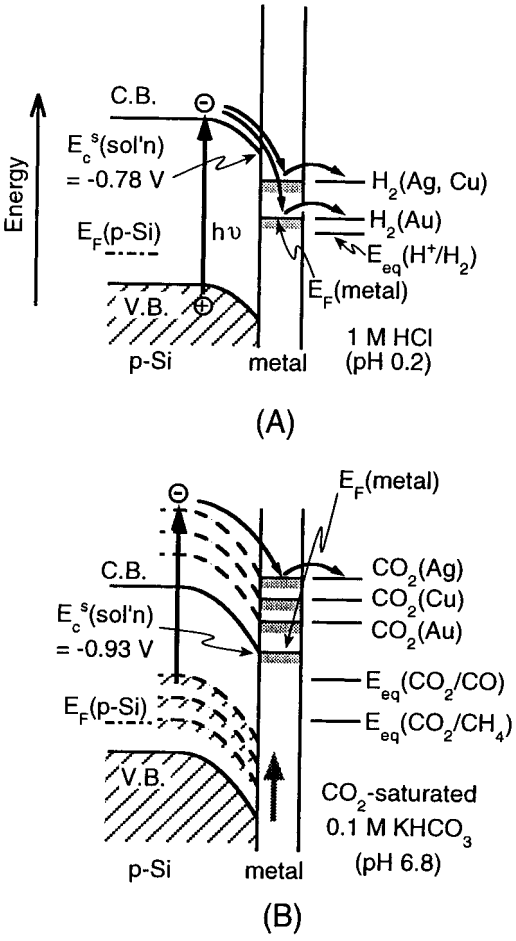

Figure 8. Energy band diagrams explaining the photoeffect of particulate-metal/p-Si: (A) for hydrogen evolution in 1.0 M HCl (pH 0.2) and (B) for CO_2 reduction in CO_2-saturated 0.1 M $KHCO_3$ (pH 6.8). Horizontal lines in solution phase, denoted by H_2(Au), CO_2(Au), etc., represent the observed onset potentials of the H_2 evolution and CO_2 reduction on the metal electrodes indicated in the parentheses. $E_{eq}(H^+/H_2)$ is the equilibrium potential for hydrogen evolution at pH 0.2 and $E_{eq}(CO_2/CO)$ and $E_{eq}(CO_2/CH_4)$ are those for the CO_2 reduction to CO and CH_4 at pH 6.8, respectively. $E_C{}^S$(soln), E_F(metal), and E_F(p-Si) have the same meaning as those in Figure 6. See text for details.

photovoltage of 0.5 V. Such an apparent contradiction between the hydrogen evolution and CO_2 reduction can be explained by taking into account the difference in the reduction potentials for the reactions.

The conduction and valence band edges at the naked p-Si surface in 1.0 M HCl are estimated to be −0.78 V and +0.34 V vs SCE, from the flat-band potential of n-Si (−0.62 V)[13,31,32] in 1.0 M HCl together with the band gap of Si (1.12 eV) and the energy difference (0.16 eV) between the Fermi level and the bottom of the conduction band for n-Si ($N_D = 6.4 \times 10^{14}$ cm^{-3}). Thus, the onset potentials for the H_2 evolution on the Cu, Ag, and Au metal electrodes (−0.60, −0.57, and −0.35 V, respectively, as taken from the potentials of $j = 1.0$ $mAcm^{-2}$) are all below the conduction band edge of the naked p-Si surface, as shown in Figure 8A. This implies that photogenerated electrons can move to the metal particles and cause hydrogen evolution without any shift of the p-Si band edges for all the particulate-metal/p-Si electrodes. In other words, the onset potentials of hydrogen-evolution photocurrent for the particulate-metal/p-Si are solely determined by the flatband potential of the naked p-Si, independent of the difference in the onset potentials for hydrogen evolution on the deposited metals, and agree with each other as really observed (Figure 7A).

On the contrary, the onset potentials of the CO_2 reduction on the Cu, Ag, and Au electrodes (−1.30, −1.45, and −1.15 V, respectively) are far above the conduction band edge of the naked p-Si surface in CO_2-saturated 0.1 M $KHCO_3$ of pH 6.8 (ca. −0.93 V vs SCE, the flat-band potential of n-Si does not shift at a ratio of 0.059 V/pH but shifts at 0.023 V/pH in the pH range below 7[31,32]), though the equilibrium potentials for the CO_2 reduction to CO, CH_4, and C_2H_4 are −0.75, −0.48, and −0.56 V vs SCE at pH 6.8, respectively, and below the conduction band edge of the naked p-Si (Figure 8B). Thus, the CO_2 photoreduction on the particulate-metal/p-Si can occur only when the surface band energies of p-Si as well as the Fermi level of the metal particles are shifted upward to some extent as shown in Figure 8B. Such an upward shift is achieved by accumulation of electrons at the p-Si surface as well as in the metal particles, accompanied by changes in potential drops in the Helmholtz layers at the p-Si and metal-particle surfaces. The accumulation of electrons continues until the conduction band edge of the p-Si surface and the Fermi level of the metal particles reach the onset potentials of the CO_2 reduction on the metal particles. Therefore, the onset potentials of photocurrents for the CO_2 reduction on the particulate-metal/p-Si depend on the kind of the deposited metals. This argument implies that the present type semiconductor electrode has an ability to shift its surface band energies so as to get good energy-level matching between the semiconductor and solution reactants, similar to naked semiconductor electrodes. This is in sharp contrast to

behavior of molecular (and particulate semiconductor) photocatalysts.[33,34]

From the arguments made so far, we can conclude that the electrode of the present type (Figure 1) can in principle meet all the requirements for high efficiency, mentioned in the Introduction section and become an ideal type electrode for the CO_2 photoreduction. Now let us consider the surface structure of actual electrodes as compared with the model electrode of Figure 1A. The size of deposited metal particles seen in the SEMs (20−200 nm, Figure 2) is considerably larger than the theoretically expected optimum value (ca. 5 nm)[9,10] and the particle density is high in the case of Au (Figure 2C), nevertheless a high photovoltage of 0.5 V is generated. This is most probably due to the fact that the areas of direct metal/Si contacts are much smaller than the particle size seen in the SEMs, the electrolyte partly penetrating into the metal-particle/Si interface, such as shown in Figure 1B. This expectation is supported by the aforementioned fact that the increase in the electricity of metal particle deposition only increased the particle size, not affecting the particle density. This fact implies that the metal deposition occurs only on metal nuclei formed on certain active site of the p-Si surface at the initial stage of the electrodeposition, and thus the metal particles are in direct contact with p-Si only in the small areas of the initial metal nuclei. The small areas of the direct Si/metal contact may also be caused by geometrically rough structure of concentrated-HF-etched p-Si surfaces on a few nanometer scale as revealed by recent STM studies.[35] Thus we can say that the actual electrodes (Figure 1B) have essentially the same metal-contact structure as the model electrode of Figure 1A.

The photovoltage of 0.5 V obtained in the present work is a little smaller than the open-circuit photovoltages of 0.62 to 0.64 V obtained for metal-particle-coated n-Si-based PEC solar cells.[9−12] A possible reason may lie in that the areas of direct metal/Si contacts in the present work are still too large for some metal particles, leading to a decrease in the photovoltage. Another possible reason is that H^+ ions penetrate into the interior of p-Si, resulting in interstitial H atoms,[36] which act as a recombination center. These discussions indicate that the control of surface structure not only on an atomic scale but also on a nanometer-sized level is important for getting a higher efficiency.

The Cu, Ag, and Au metals used in the present work are the most active electrocatalysts for the CO_2 reduction for the present, but the onset potentials of the CO_2-reduction are still considerably more negative than the equilibrium potentials and hence above the conduction band edge of p-Si (Figure 8B). For this reason, however, the Fermi level of metal particles can coincide with the conduction band edge in a stationary state under illumination (Figure 8B), leading to the formation of the highest energy barrier height. Though it does not seem to be easy to find more active metallic electrocatalysts for the CO_2 reduction, if they are found, they will shift the onset potentials of the CO_2 reduction close to the equilibrium potentials and below the conduction band edge of p-Si. For such a case, the high energy barrier can be obtained either by a downward shift of the conduction band edge of p-Si (e.g., through the formation of Si−F termination bonds[37]) or by using another semiconductor having an appropriate conduction band edge.

Acknowledgment. The present work was partly supported by a Grant-in-Aid for Scientific Research on Priority Areas of the Ministry of Education, Science, Sports and Culture (Grant 09237105).

References and Notes

(1) Yoneyama, H.; Sugimura, K.; Kuwabata, S. *J. Electroanal. Chem.* **1988**, *249*, 143.
(2) Bockris, J. O.; Wass, J. C. *J. Electrochem. Soc.* **1989**, *136*, 2521.
(3) Taniguchi, I. In *Modern Aspects of Electrochemistry*; Bockris, J. O., White, R. E., Conway, B. E., Eds.; Plenum: New York, 1989; Vol. 20, Chapter 5.
(4) Noda, H.; Ikeda, S.; Saito, Y.; Nakamura, T.; Maeda, M.; Ito, K. *Denki Kagaku* **1989**, *57*, 1117.
(5) Ikeda, S.; Saito, Y.; Yoshida, M.; Noda, H.; Maeda, M.; Ito, K. *J. Electroanal. Chem.* **1989**, *260*, 335.
(6) Flaisher, H.; Tenne, R.; Halmann, M. *J. Electroanal. Chem.* **1996**, *402*, 97.
(7) Junfu, L.; Baozhu, C. *J. Electroanal. Chem.* **1992**, *324*, 191.
(8) Hashimoto, K.; Fujishima, A. *Spec. Publ. R. Soc. Chem.* **1994**, *153*, 388 *(Carbon Dioxide Chemistry: Environmental Issues)*.
(9) Nakato, Y.; Ueda, K.; Yano, H.; Tsubomura, H. *J. Phys. Chem.* **1988**, *92*, 2316.
(10) Nakato, Y.; Tsubomura, H. *Electrochim. Acta* **1992**, *37*, 897.
(11) Yae, S.; Nakanishi, I.; Nakato, Y.; Toshima, N.; Mori, H. *J. Electrochem. Soc.* **1994**, *141*, 3077.
(12) Jia, J.-G.; Fujitani, M.; Yae, S.; Nakato, Y. *Electrochim. Acta* **1996**, *42*, 431.
(13) Nakato, Y.; Yano, H.; Nishiura, S.; Ueda, T.; Tsubomura, H. *J. Electroanal. Chem.* **1987**, *228*, 97.
(14) Kobayashi, H.; Mizuno, F.; Nakato, Y.; Tsubomura, H. *J. Phys. Chem.* **1991**, *95*, 819.
(15) Hori, Y.; Kikuchi, K.; Suzuki, S. *Chem. Lett.* **1985**, 1695.
(16) Noda, H.; Ikeda, S.; Oda, Y.; Imai, K.; Maeda, M.; Ito, K. *Bull. Chem. Soc. Jpn.* **1990**, *63*, 2459.
(17) Hinogami, R.; Mori, T.; Yae, S.; Nakato, Y. *Chem. Lett.* **1994**, 1725.
(18) Hinogami, R.; Nakamura, Y.; Yae, S.; Nakato, Y. *Appl. Surf. Sci.* **1997**, *121/122*, 301.
(19) Kobayashi, H.; Ishida, T.; Nakato, Y.; Tsubomura, H. *J. Appl. Phys.* **1991**, *69*, 1736.
(20) Morinaga, H.; Futatsuki, T.; Ohmi, T.; Fuchita, E.; Oda, M.; Hayashi, C. *J. Electrochem. Soc.* **1995**, *142*, 966.
(21) Morinaga, H.; Suyama, M.; Ohmi, T. *J. Electrochem. Soc.* **1994**, *141*, 2834.
(22) Chyan, O. M. R.; Chen, J.-J.; Chien, H. Y.; Sees, J.; Hall, L. *J. Electrochem. Soc.* **1996**, *143*, 92.
(23) Sze, S. M. *Physics of Semiconductor Devices*, 2nd ed.; John Wiley and Sons: New York, 1981; p 291.
(24) Chen, C.; Frese, K. W., Jr. *J. Electrochem. Soc.* **1992**, *139*, 3243.
(25) Chen, C.; Frese, K. W., Jr. *J. Electrochem. Soc.* **1993**, *140*, 1355.
(26) Hori, Y.; Murata, A.; Takahashi, R. *J. Chem. Soc., Faraday Trans. 1* **1989**, *85*, 2309.
(27) Kyriacou, G.; Anagnostopoulos, A. *J. Electroanal. Chem.* **1992**, *322*, 233.
(28) Hori, Y.; Wakebe, H.; Tsukamoto, T.; Koga, O. *Surf. Sci.* **1995**, *335*, 258.
(29) Takahagi, T.; Ishitani, A.; Kuroda, H. *J. Appl. Phys.* **1991**, *69*, 803.
(30) Yablonovitch, E.; Allara, D. L.; Chang, C. C.; Gmitter, T.; Bright, T. B. *Phys. Rev. Lett.* **1986**, *57*, 249.
(31) Nakato, Y.; Ueda, T.; Egi, Y.; Tsubomura, H. *J. Electrochem. Soc.* **1987**, *134*, 353.
(32) Madou, M. J.; Loo, B. H.; Frese, K. W.; Morrison, S. R. *Surf. Sci.* **1981**, *108*, 135.
(33) Ishida, H.; Terada, T.; Tanaka, K.; Tanaka, T. *Inorg. Chem.* **1990**, *29*, 905.
(34) Kanemoto, M.; Shiragami, T.; Pac, C.; Yanagida, S. *J. Phys. Chem.* **1992**, *96*, 3521.
(35) Itaya, K.; Sugawara, R.; Morita, Y.; Tokumoto, H. *Appl. Phys. Lett.* **1992**, *60*, 2534.
(36) Mierry, P. de; Etcheberry, A.; Aucouturier, M. *J. Appl. Phys.* **1991**, *69*, 1099.
(37) Fujitani, M.; Hinogami, R.; Jia, J.-G.; Ishida, M.; Morisawa, K.; Yae, S.; Nakato, Y. *Chem. Lett.* **1997**, 1041.